Time resolved stereo PIV of shock oscillations on an airfoil in transonic flow

A. Hartmann, M. Klaas, W. Schröder
Institute of Aerodynamics, RWTH Aachen University Germany,
a.hartmann@aia.rwth-aachen.de

Abstract

Time resolved stereo particle-image velocimetry (TR-SPIV) and unsteady pressure measurements are used to analyze the unsteady flow over a supercritical DRA-2303 airfoil in transonic flow. The dynamic shock wave boundary-layer interaction is a most essential feature of this unsteady flow causing a distinct oscillation of the flow field. Results from wind tunnel experiments with a variation of the freestream Mach number at Reynolds numbers ranging from 1.2 to 1.4 x 10^7 m^{-1} are analyzed regarding the origin and nature of the unsteady shock boundary-layer interaction. TR-SPIV results are presented for a weak shock strength and incipient separation as well as for a medium shock strength and full scale trailing edge separation. The time-resolved visualization of the shock wave oscillation demonstrates the two-fold nature of separated flow, first being the origin of aerodynamic unsteadiness when marginal separation occurs and second, the damping of the fluctuation level at a full-scale separation.

1. INTRODUCTION

The flow field of modern supercritical airfoils in transonic flow is characterized by a local supersonic region on the upper surface terminated by a shock wave. A highly complex and unsteady flow pattern may develop in the direct vicinity of the surface, e.g., a shock-induced separation of the turbulent boundary layer may occur. Moreover, the time dependent interaction of the shock wave with the boundary layer in the transonic flight regime may lead to an oscillation of the shock wave generating pressure fluctuations acting on the wing structure as time-dependent load distribution. Hence, wings of modern transport aircraft with optimized light-weight design may exhibit a distinctive structural response to unsteady loads.
To understand this phenomenon series of wind-tunnel tests have been conducted with the supercritical laminar type airfoil DRA-2303. The experiments have been performed in a transonic intermittent vacuum-storage wind tunnel at freestream Mach numbers between M_∞ = 0.64 and 0.76 and angles of attack between α = 0° and 3°. The airfoil flow exhibits an increased degree of unsteadiness at a Mach number range between M_∞ = 0.70 and 0.73 and angles of attack between α = 1° and 3° due to a dynamic interaction between the shock wave and the turbulent boundary layer, eventually causing a steady trailing-edge separation.
Flow field information is obtained using three-component time resolved stereo particle-image velocimetry (TR-SPIV) to capture any three-dimensional characteristics present in the flow field. The resolution of Furthermore, steady and unsteady pressure measurements as well as high-speed Schlieren imaging have been applied. The results from the experimental test campaigns will also be used to assess the accuracy and validity of a numerical simulation of the unsteady shock boundary-layer interaction.

2. EXPERIMENTAL SETUP

The experimental investigation has been conducted in the Trisonic Wind Tunnel of the RWTH Aachen University. This facility is an intermittently working vacuum storage tunnel producing flows at Mach numbers ranging from 0.4 to 3.0. Depending on the Mach number, the entire test run lasts about 10 seconds with 2-3 seconds of stable flow with a turbulence intensity below 1 % [1]. For transonic flows with freestream Mach numbers below one, the tunnel is equipped with a 0.4 m x 0.4 m two-dimensional adaptive test section consisting of parallel side walls and flexible upper and bottom walls to simulate unconfined flow conditions [2]. The wall contours are calculated by the one-step method solving the Cauchy integral based on the time-averaged pressure distribution measured along the center line of the flexible walls [3]. The total pressure and temperature of the wind tunnel are determined by the ambient conditions. Therefore, the Reynolds number depends on the Mach number and ambient temperature ranging from 1.2 to 1.4 x 10^7 m^{-1} in the present experiments. The relative humidity of the flow is kept below 4 % at total temperatures of about 293 K to exclude any influence on the shock wave position [4]. The
The acoustic environment in the wind tunnel is of major interest for the experimental simulation of dynamic fluid interaction processes. For this reason, the adaptive test section is equipped with 26 dynamic pressure transducers distributed along the center line of the upper and lower wall. The freestream chamber located downstream of the test section is identified as the main source of acoustic disturbances in the test section, since spectral powers of the pressure transducers always peak in the wall locations closest to this area. Depending on the freestream Mach number, the acoustic disturbances contain three predominant frequencies, most likely evolving from different acoustic modes in the freestream chamber. The fluctuation power contained in the modes also depends on the Mach number. When analyzing the results of the measurements of the flow over the airfoil model, the influence of the test section acoustics has to be taken into account.
The airfoil model comprises the supercritical laminar type profile DRA-2303 which has been under investigation in the Euroshock project [5]. The airfoil has a relative thickness to chord ratio of 14 % and a chord length of c = 200 mm. The laminar-turbulent transition of the boundary layer is fixed at 5 % chord using a 117 µm zigzag shaped transition strip. The model is equipped with

11 Kulite XCQ-080 subminiature pressure transducers in the area of the shock boundary-layer interaction ranging from x/c = 0.45 - 0.7 on the upper surface. The distance

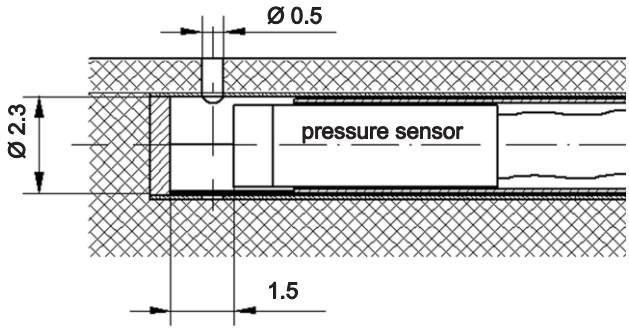

Figure 1. Pressure transducer installation

between the pressure taps is 0.05 x/c. Each transducer is installed in closest proximity to the corresponding pressure orifice to minimize the damping and phase shift of the measured pressure signal against the actual signal on the airfoil surface (Fig. 1). Figure 2 shows the dynamic response of the sensor installation plotted against the reduced frequency $\omega^* = 2\pi fc/u_\infty$ in the Mach number range of $0.8 \le M \le 1.4$ relevant for the flow conditions under consideration. The response function was calculated using the theory developed by Bergh and Tijdeman [6] for the propagation of small harmonic pressure perturbations through tube-transducer systems. The calculations show that the response function has a very small influence on pressure fluctuations in the reduced frequency range of $\omega^* < 3$ of the flow field oscillation which is investigated in this study.

Nevertheless, the phase shift ϕ_u/ϕ_i and the gain p_u/p_i are considered for the data evaluation, using a first order approximation for the transfer function developed by Bergh and Tijdeman. In figure 2, the approximation of the transfer function is compared to the original function for M = 1 showing the validity of the approximation for the relevant frequency range of $\omega^* < 3$. The approximation allows to calculate the original pressure value p_u at the pressure orifice using the following equation (1)

$$p_u = p_i + Tp_i' \quad (1)$$

with T being the time constant which is determined for each Mach number using the original transfer function and p_i being the pressure value at the pressure sensor.

The pressure transducer signals are recorded by a data acquisition (DAQ) system consisting of five data acquisition boards Imtec T-112 with simultaneous analog-to-digital conversion of 40 channels, 12 bit resolution, and up to 1.25 MHz sampling rate per channel. In the present experiments, a sampling rate of f_s^{DAQ} = 20 kHz was selected. The signals are conditioned with 4-pole Butterworth low-pass filtering with 10 kHz corner frequency and hundredfold amplification with a bandwidth of 100 kHz by Endevco 136 DC-amplifiers.

For steady pressure measurements the model comprises 25 pressure taps on the upper surface and 19 pressure taps on the lower surface.

In addition to pressure measurements, three-component time-resolved stereo particle-image velocimetry (TR-SPIV) with the laser light sheet positioned parallel to the incoming flow has been employed to analyze the flow field from x/c = 0.4 - 0.9 on the test section center line. Droplets of Di-Ethyl-Hexyl-Sebacat (DEHS, CAS-No. 122-62-3) were used as seeding with a mean diameter of 0.6 µm as per datasheet of the Topas GmbH ATM 242 atomizer. To achieve a homogenous seeding distribution, the seeding was added to the flow in the dry air reservoir of the wind tunnel prior to each test run. The particle response time τ_p can be calculated to be approximately 1.98 µs using the approach by Melling [7] corresponding to a frequency response of f_p = 505 kHz.

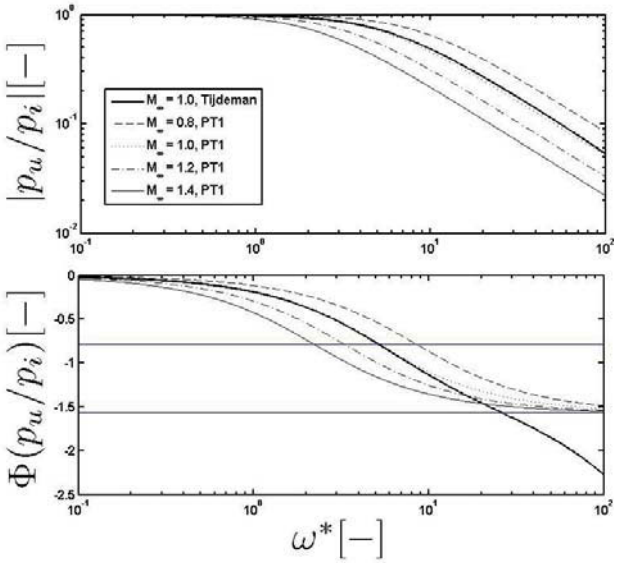

Figure 2. Modulus and phase of sensor installation dynamic response as a function of the reduced frequency ω^* for $0.8 \le M \le 1.4$

The flow was illuminated using a Quantronix Darwin Duo 40M double-pulsed Nd:YLF laser with a wavelength of 527 nm. The repetition rate was set to 1500 Hz resulting in an energy of approximately 15 mJ per pulse. The thickness of the laser light sheet was about 1 mm. The optical access for the laser beam was provided through an aperture in the freestream chamber of the wind tunnel downstream of the test section. Using the frame-straddling technique mentioned by Raffel et al. [8] the laser pulse separation in the experiments was 3.4 µs leading to a mean particle displacement of approximately 1 mm corresponding to approximately 10 pixel in the acquired flow images. The particle images were recorded with two Photron Fastcam SA-3 CMOS cameras in Scheimpflug condition with a viewing angle of 36°. Both cameras record the forward scatter of the particles as shown in figure 3. The cameras are equipped with a 1024 x 1024 pixel sized sensor capable to achieve a frame rate of 2000 Hz at full resolution. The sensor was cropped to 1024 x 512 pixels to achieve an increased recording rate of 3000 Hz leading to a sampling rate of f_s^{PIV} = 1500 Hz. This frequency is six times higher than the highest frequency of the shock oscillation measured with the Kulite pressure transducers, though fulfilling the Nyquist criterion. Furthermore, the spectra achieved from the TR-SPIV measurements perfectly agree with the pressure spectra obtained with 20 kHz such that we define the SPIV measurements as time resolved regarding the shock wave oscillation. Two 100 mm Tokina 1:2.8 macro lenses were mounted to the cameras. The optical settings result in a particle diameter of

approximately 3 pixel in the recorded images. The resulting field of view covers the airfoil surface from x/c = 0.38 to 0.85 and reaches from the wing surface to y/c = 0.2. Figure 3 depicts an overview of the test setup.
In each test run a dataset of 2726 image pairs was acquired. The images were analyzed with ILA VidPIV software. Prior to the evaluation, the images of each camera were dewarped using the information of a calibration target placed into the light sheet plane. This perspective mapping of the images is done by a Tsai-model [9] which is based on the pin-hole model of perspective projection. Due to a misalignment of the calibration target with respect to the laser light sheet, a certain error cannot be excluded in the reconstruction of the third velocity component from the two component vector fields. This error can be corrected by determining the local misalignment using the approach of Willert [10] by calculating a so called disparity map. The disparity map is used to improve the mapping functions so that the final disparity is minimized. The dewarped and disparity corrected images are evaluated using adaptive cross-correlation with window shifting and deformation schemes. A final window size was 32 x 32 pixel with an overlap factor of 50 %. This leads to a resolution of 1.50 mm with 98 % of valid vectors. For post-processing, a window velocity and a local median filter have been used to identify and remove outliers. Then, the stereoscopic reconstruction is applied to calculate the third velocity component. Again, the reconstruction is based on the parameters of the Tsai-model. To remove spurious vectors, the third velocity component is locally filtered after the reconstruction.

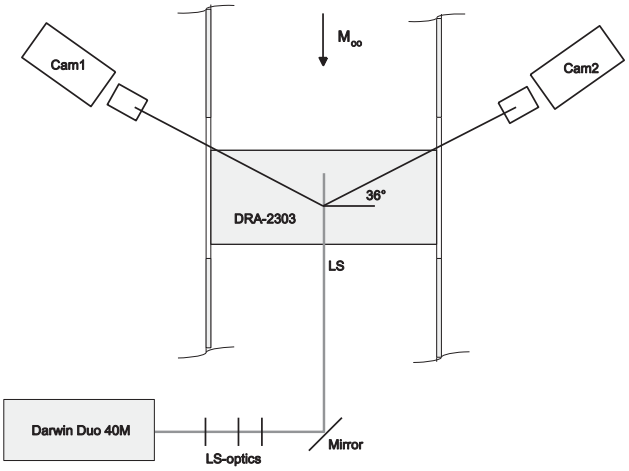

Figure 3. Overview of the TR-SPIV setup

For the synchronization of the TR-SPIV and the time-resolved pressure measurements, the exposure signal of the camera of each frame was recorded with the DAQ system used for the pressure transducer signals leading to a maximum time discrepancy of 25 µs due to the different recording rates of 3 and 20 kHz, respectively.
Exposure tests with the Nd:YLF high speed laser with 15 mJ pulse energy showed a significant local heating of the airfoil surface in the area illuminated by the laser light sheet due to absorption of the araldite gel coat layer. To avoid any deterioration of the surface quality and structural stiffness, a 10 mm wide and 0.2 mm thick 3M aluminum tape is integrated into the wing surface. The tape, which serves as thermal barrier coating, is flush-mounted by applying it onto the surface during the model manufacturing process to avoid any surface distortion.
Due to the limited spatial extension of the PIV measurement plane, high speed Schlieren imaging (HSI) has been applied to qualitatively visualize the integral density gradient distribution of the entire flow field on the upper surface of the airfoil. It has been applied synchronously with unsteady pressure measurements mentioned above. The Schlieren technique employs a standard Z-type Schlieren setup [11]. The Schlieren images were recorded with a Photron SA-3 high-speed camera described above. The recording rate was set to f_s^{HSI} = 3000 Hz.

3. RESULTS

In the following, time averaged and time resolved results obtained from the wind-tunnel measurements will be presented. It is obvious that wind-tunnel investigations quantitatively cannot be of general nature regarding real flow cases, but are useful to gather a general understanding of the phenomenon also providing a reference case for comparison with numerical simulations with respect to the related wind tunnel.

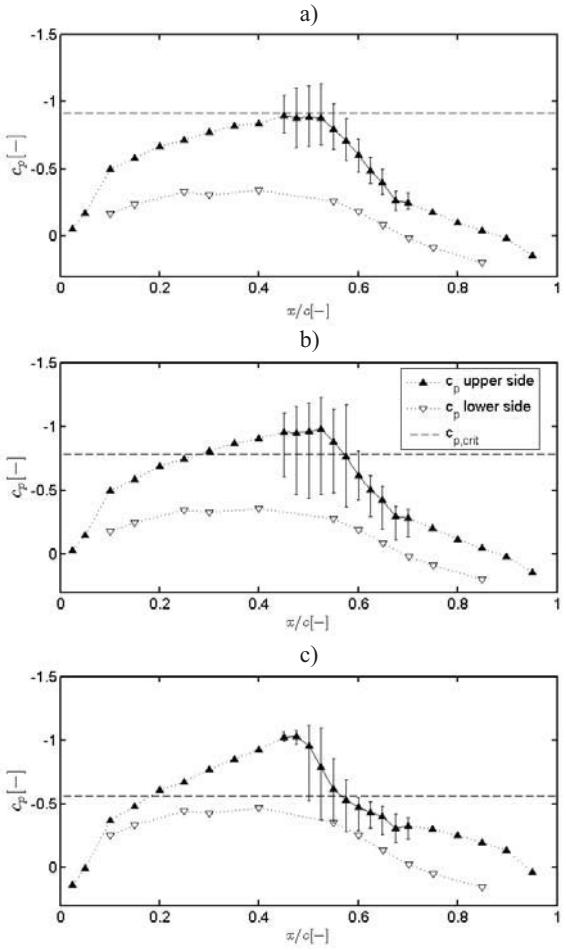

Figure 4. Time averaged pressure distribution for α = 1° and M_∞= 0.67 (a), M_∞= 0.70 (b), and M_∞= 0.76 (c)

3.1. Time Averaged Flow Analysis

The unsteady aerodynamic flow field of the airfoil is dominated by flow characteristics, which are accessible to

time averaged flow measurement tools. The time airfoil aerodynamics has been investigated for angles of attack ranging from α = 0° to 3°, freestream Mach numbers between M_∞ = 0.64 and 0.76, and Reynolds numbers Re_∞ related to the aerodynamic chord c in the order of 10^6. The main feature of the transonic airfoil flow is a compression shock terminating the supersonic bubble in the flow field. Figure 4 exemplarily displays the time averaged pressure distribution for M_∞ = 0.67, 0.70, and 0,76, respectively, for an angle of attack α = 1°. At M_∞ = 0.70 and 0.76 the steep pressure rise normally indicating a weak shock wave is smoothed by the time averaging. The unsteadiness of the flow is shown by the length of the error bars denoting the global maximum and minimum measured with the 11 unsteady pressure transducers during the testing time. The supersonic flow area grows at increasing freestream Mach number leading to a stronger shock which evolves closer to the trailing edge. At M_∞ = 0.76 the appearance of a strong shock marks the change from a mild to a severe interaction with the boundary layer, which is consistent with the commonly known Mach number effect on the transonic flow field described by Seddon [12], Green [13], Adamson & Messiter [14], and Délery [15,16].

3.2. Time Resolved Flow Analysis

3.2.1. Pressure distribution

The time averaged flow analysis provides an insight in the global flow features, but does not give information of the temporal development of specific flow patterns, e.g., the oscillation of the shock wave. This, for instance, has been already illustrated by the smoothing effects contained in the pressure distributions caused by flow unsteadiness (Figure. 4). Nevertheless, the airfoil flow field exhibits a strong streamwise oscillation in the position of the shock wave. The strongest surface pressure fluctuations can be found in the region of the time averaged shock position and in the area downstream of the shock, caused by the interaction with the boundary layer. The spectra of pressure signals for the shock free flow case at $[\alpha, M_\infty]$ = [1°,0.67] contain distinct harmonic peaks in ω^* = 0.66 and 1.43 illustrating the periodic nature of the flow (Fig. 5a). As soon as the shock pattern occurs, the frequency of 1.38 dominates the flow field (Fig 5b) with distinct higher harmonics present (e.g. ω^* = 2.76). At $[\alpha, M_\infty]$ = [1°,0.76], the fluctuations become significantly smaller at a frequency of ω^* = 1.29 (Fig 5c). The spectrograms presented in Fig. 5 are representative in quality for the entire upper surface. Periodic shock oscillations have been investigated in several experimental and numerical studies. Brunet et al. [17] describe a “pulsation” of the separated area to be the origin of buffet oscillations on the OAT15A supercritical airfoil with a thickness to chord ratio of 12.5%. In his widely accepted shock buffet model, Lee [18] describes the inviscid shock interaction with upstream propagating sound waves, which are generated by the impingement of large scale turbulent eddies on the sharp trailing edge forming a feedback loop with disturbances convected downstream, as the main buffet mechanism [19]. A reduced buffet frequency of ω^* = 0.55 was measured by Schewe et al. [20] for the NLR-7301 airfoil. Finke [21] and Lee [18] measured shock buffet frequencies of ω^* = 0.5 to

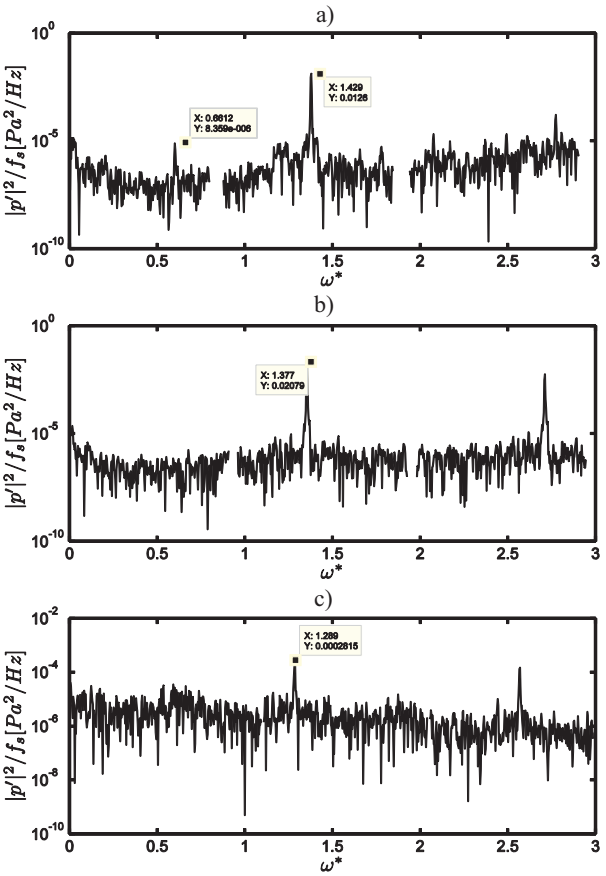

Figure 5. Power spectral analysis of the pressure signal at x/c = 0.55 for α = 1° and M_∞= 0.67 (a), M_∞= 0.70 (b), and M_∞= 0.76 (c)

No. 1 airfoil with a relative thickness of 11.8%. Hence, the measured reduced buffet frequency of ω^* = 1.38 at M_∞= 0.70 on the DRA-2303 airfoil is in the range of other supercritical airfoils with a comparable thickness ratio and shock position. However, a reduced Buffet frequency of $\omega^* \approx$ 0.65 at M_∞= 0.702 and α = 2.4° has been measured for the DRA-2303 airfoil in the Euroshock project [5]. Furthermore, the normalized frequency of the oscillation slightly changes with the number M_∞ and the true value remains almost constant at 248 Hz. This frequency is also present in the spectrum of the shock-free flow case at M_∞= 0.67 (Figure 4, 5). This evidences that the frequency of the shock wave oscillation is dominated by wind tunnel resonance that forces the natural shock wave oscillation of the airfoil to lock-in to this resonance frequency or that excites a higher mode of the natural oscillation. Such a behavior has been predicted in a computational study by Raveh et al. [22] in terms of a forced pitching oscillation of a NACA 0012 airfoil. In Figure 4 c) it becomes obvious that the RMS values of the pressure transducers located upstream of the shock wave significantly decrease for the flow cases at M_∞ = 0.76 where a strong shock wave is present. This strengthens the theory that the disturbances generated in the freestream chamber downstream of the test section cause the present shock wave oscillation and that they are low-pass filtered by the shock wave. A filtering effect of shock waves has been reported for high frequency disturbances in the boundary layer upstream of the shock wave e.g. by Dussauge [23].

In the case of classical buffet, the shock is strong enough to cause a fully separated flow between the shock boundary-layer interaction area and the trailing edge. The formation of the acoustic feed-back loop can be observed at high Mach numbers and high angles of attack. In the DRA-2303 buffet flow considered here, the trailing edge separation itself is disturbed by the tunnel unsteadiness and leads to an oscillatory shock motion only due to the local interference between the shock foot and the separation line. Hence, the flow at higher Mach numbers, in the present case at M_∞ = 0.76, can be considered as a flow, where almost no shock buffet occurs due to the higher shock strength governing the separation. The existence of a steady flow case at higher Mach numbers is also described by Xiao [24] on an 18% thick circular arc airfoil and by Geissler [25] for the NLR 7301 airfoil in the context of numerically simulating limit cycle oscillations.

3.2.2. Velocity distribution

To gain information on the velocity field, TR-SPIV is used to visualize the unsteady flow around the DRA 2303 airfoil in the vicinity of the shock boundary-layer interaction zone. The vertical measurement plane is located along the center line of the adaptive test section and orientated in the streamwise direction. Figure 6 depicts a combination of an instantaneous velocity field measured with TR-SPIV and the respective pressure distribution and the density gradient in the flow field from Schlieren imaging at $[\alpha, M_\infty]$ = [1°,0.76]. The image evidences the location of the TR-SPIV measurement plane and gives an overview of the surrounding flow field. The three measurement techniques agree in terms of the shock wave location and the extension of the shock induced rear separation present in this flow case.

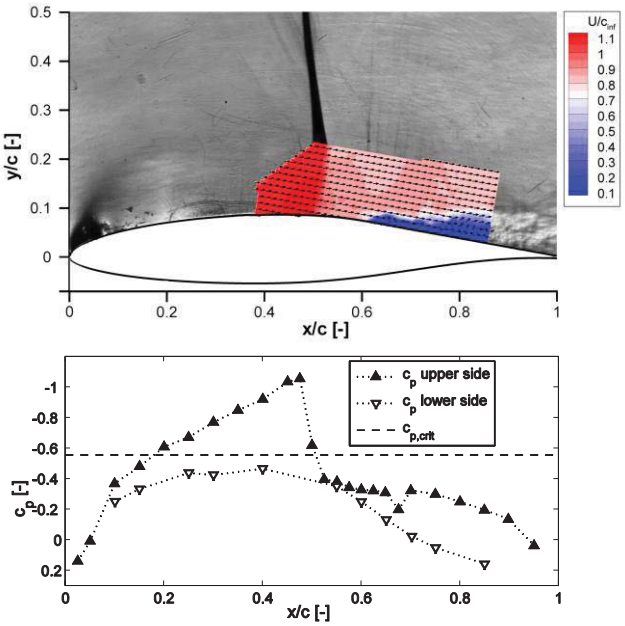

Figure 6. Instantaneous velocity, density gradient, and pressure distribution at α = 1° and M_∞= 0.76

In the following, TR-SPIV results are presented together with the synchronous pressure distribution in the range of

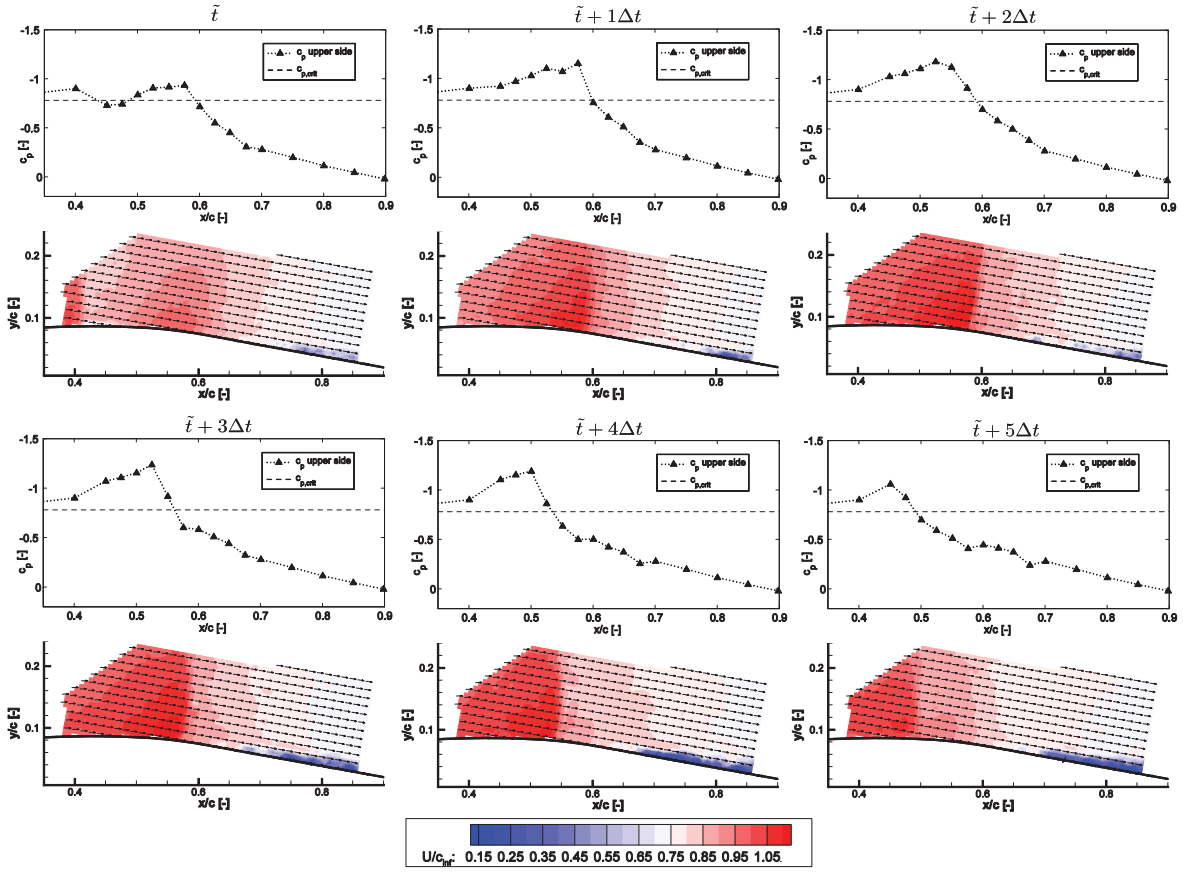

Figure 7. Representative time sequence of synchronously measured pressure distribution and velocity field for α = 1°, M_∞ = 0.70, Re_∞ = 2.66x10^6, time step Δt = 0.67 ms

x/c = 0.4 - 0.9.Due to the fact that the third velocity component is very small compared to the x- and y-components, only the absolute velocity values are presented. Figure 7 shows a representative time sequence of the synchronized pressure distribution and velocity field acquired with f_s^{PIV} = 1500 Hz, i.e., a time-step Δt = 0.67 ms, at $[\alpha_0, M_\infty]$ = [1°,0.70]. Note that pressure values upstream of x/c = 0.45 and downstream of x/c = 0.7 are time averaged. Every second velocity vector is plotted. Consistent with the results from the unsteady surface pressure measurement, a large-scale streamwise shock oscillation occurs on the upper wing surface. At time $t = \tilde{t}$, figure 7 shows the shock wave located in its mostforward position at x/c = 0.4. At this time step, the shock wave has almost vanished which is followed by an expansion downstream of the shock wave. A second supersonic flow region which is closed by a weak shock wave is formed. The development of this second region marks the beginning of the cycle. One time-step later at $t = \tilde{t} + 1\Delta t$, the second region has grown significantly, in terms of both, spatial extension as well as strength, and at $t = \tilde{t} + 2\Delta t$, it is fully developed. In the following at $t = \tilde{t} + 3\Delta t$, the supersonic region starts to shrink. This shrinking is accompanied by an accelerating motion of the shock wave into the upstream direction. During this upstream shock motion, the supersonic flow field loses its strength resulting in a weakening of the shock wave up to a point where the cycle starts again and a new supersonic region develops.

At time-steps $t = \tilde{t}$ and $\tilde{t} + 1\Delta t$, an incipient rear separation of the boundary layer can be seen far downstream of the shock wave. At the following three time steps the separation line is consistent with the location of the shock wave caused by the stronger pressure gradient across the shock. The separation line again is located downstream of the shock position at $\tilde{t} + 5\Delta t$, meaning that the shock wave is already too weak to cause the boundary layer to separate. The identification of the separation line is consistent with the data of the Schlieren imaging and can be done more precisely using the raw images of the TR-SPIV measurements. The subcritical flow field on the upper side is also determined by a separation of the boundary layer at the trailing edge. The separation occurs in the area of the positive pressure gradient growing upstream with increasing Mach numbers to finally coincide with the shock position as soon as the shock is strong enough to induce separation. This flow development resembles the type B3 flow in the phenomenological description given by Pearcey et al. [26].

Quasi-harmonic large scale shock motions were first categorized by Tijdeman [27]. An intermittent presence of the shock wave comparable to the flow behavior observed in the present study is described as Tijdeman type B shock motion. In this category, however, the shock wave disappears during part of its backward motion, while the DRA-2303 airfoil flow shows a disappearance of the shock close to the upward end of its cycle. In Tijdeman type C motion the shock also disappears during its upward motion, but with increasing shock strength and by

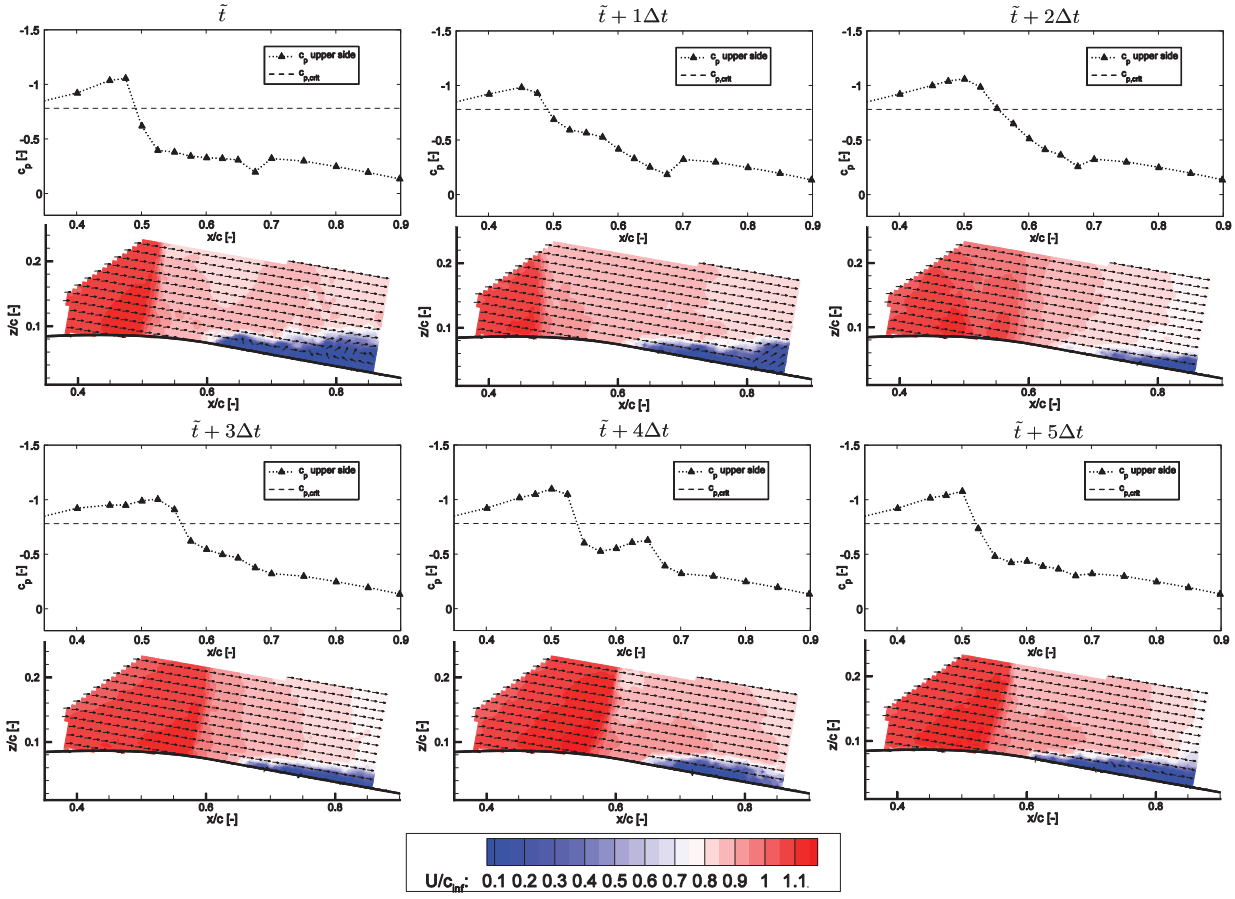

Figure 8. Representative time sequence of synchronously measured pressure distribution and velocity field for α = 1°, M_∞ = 0.76, Re_∞ = 2.79x10^6, time step Δt = 0.67 ms

propagating upstream as a sound wave into the incoming flow. The shock motion phenomenon on the DRA-2303 airfoil is quite different from the Tijdeman description, since the supersonic region decreases in strength to cause the also weakening shock wave to disappear during its upward motion.

The situation changes at $[\alpha, M_\infty]$ = [1°,0.76], since the supersonic flow is generally stronger here. Therefore, in figure 8, the shock wave is present during the entire oscillation cycle, while the variation in strength of the supersonic field is generally smaller. Compared to the flow field at $[\alpha, M_\infty]$ = [1°,0.70] the velocity field at M_∞ = 0.76 also shows a significant difference in flow behavior regarding the trailing edge separation. In the former case, the separation originates in closest proximity to the trailing edge and extends upstream to the instantaneous shock foot line when the shock wave is located close enough to the trailing edge, e.g., at time steps $t = \tilde{t} + 2\Delta t$ to $\tilde{t} + 4\Delta t$ in figure 7. This large scale evolution of the separation line is a strong source of unsteadiness for this flow case. In the latter case, $[\alpha, M_\infty]$ = [1°,0.76], the mean chord wise shock position can be found further downstream, thus inducing the separation during the entire oscillation cycle. This quasi-stable correlation between the shock foot position and the separation line greatly reduces the flow dynamics. The image time-series in figure 8 also evidences that the flow unsteadiness is solely contained in the pulsation of the large scale separation, which causes a time-dependent deflection of the local streamlines. Therefore, the shock oscillation appears to be only a reaction to the change in the instantaneous downstream boundary conditions. The amplitude of the shock oscillation is also reduced from 20% chord to 10% chord at $[\alpha, M_\infty]$ = [1°,0.76].

4. CONCLUSION

Results from an experimental investigation of two different transonic flows around a DRA-2303 airfoil with dynamic shock boundary-layer interaction have been presented. One flow exhibits a highly dynamic local interaction of a weak shock with a marginal trailing-edge separation, the other flow is dominated by a stronger shock wave associated with a severe but less dynamic trailing-edge separation. Time resolved stereo particle-image velocimetry was used to display the dynamic interaction between the oscillating shock wave and the separated flow in the rear part of the airfoil. The results demonstrate a significant reduction of the unsteadiness of the flow case with higher Mach number M_∞ = 0.76. The quasi-steady position of the separation line, either induced by the stronger shock wave, or being a result of the close proximity of the existing marginal trailing edge separation and the mean shock wave position, has been identified to be responsible for this phenomenon. A similar conclusion in the context of aeroelastic instabilities in transonic flow for transport type wing configurations has been drawn by Tichy [28] and Schewe et al. [29], who attributed the rising flutter stability limit towards higher flight Mach numbers to the occurrence of separated flow as a damping feature in the unsteady transonic wing aerodynamics. For future measurement campaigns with the DRA-2303 airfoil in the Trisonik Wind Tunnel, the freestream chamber will be modified by means of two additional parallel upper and lower walls to separate the flow from the chamber. First measurements have shown that the disturbances have been completely removed showing the effect of this approach. The results from this paper show the feasibility of the chosen approach to gain detailed information on such a complex flow phenomenon and will we applied to a flow case with classical buffet in the future.

5. ACKNOWLEDGMENTS

This research was funded by the Deutsche Forschungsgemeinschaft within the research project “Numerical and Experimental Analysis of Shock Oscillations at the Shock- Boundary-Layer Interaction in Transonic Flow” (SCHR 309/40-1).

6. REFERENCES

[1] Guntermann, P., „Entwicklung eines Profilmodells mit variabler Geometrie zur Untersuchung des Transitions-verhaltens in kompressibler Unterschallströmung“, Shaker Verlag, ISBN 3-86111-365-1, 1992.

[2] Romberg, H.-J.,”Two-dimensional wall adaption in the transonic wind tunnel of the AIA”, *J. Aircraft* 38 (4), 1990, pp. 177-180.

[3] Amecke, J. “Direkte Berechnung von Wandinterferenzen und Wandadaption bei zweidimensionaler Strömung in Windkanälen mit geschlossenen Wänden”, DFVLR-FB 85-62, 1985.

[4] Binion, T. W., “Potentials for Pseudo-Reynolds Number Effects. In: Reynolds Number Effects in Transonic Flow”, AGARDograph 303, sec. 4, 1988.

[5] Stanewsky, E., Delery, J., Fulker, J., de Matteis, P., “Drag Reduction by Shock and Boundary Layer Control”, Results of the Project EUROSHOCK, AER2-CT92-0049, Notes on Numerical Fluid Mechanics Vol. 56, Springer Verlag, 1997.

[6] Tijdeman, H., “Theoretical and experimental results for the dynamic response of pressure measuring systems”, NLR-TR F.238, 1965.

[7] Melling, A., “Seeding Gas Flows for Laser Anemometry, Proceedings on the Conference of Advanced Instrumentation for Aero Engine Components”, AGARD CP-399, 8.1., 1986.

[8] Raffel, M., Willert, C. E., Wereley, S. T., Kompenhans, J., “Particle Image Velocimetry – A Practical Guide”, Springer, 2007.

[9] Tsai, R. Y., “An efficient and accurate camera calibration technique for 3d machine vision”, Proceedings of IEEE conference on computer vision and pattern recognition, 1986, pp. 364-374.

[10] Willert, C., “Stereoscopic particle image Velocimetry for application in wind tunnel flows”, *Meas. Sci. Technol.*, Vol. 8, pp. 1465-1479.

[11] Tropea, C., Foss, J., Yarin, A., “Handbook of Experimental Fluid Mechanics”, Springer 2007.

[12] Seddon, J., “The flow produced by interaction of a turbulent boundary layer with a normal shock wave of strength sufficient to cause separation”, RAE TM Aero 667, R&M 3502, 1960.

[13] Green, J. E., “Interactions Between Shock Waves and Turbulent Boundary Layers”, *Progr. Aerosp. Sci.*, Vol. 11, 1970, pp. 235-340.

[14] Adamson, T. C. Jr., Messiter, A. F., “Analysis of two-dimensional interactions between shock waves and boundary layers”, *Ann. Rev. Fluid Mech.*, Vol. 12, 1980, pp. 103-138.

[15] Délery, J. M., “Shock wave / turbulent boundary layer interaction and its control”, *Progr. Aerosp. Sci.*, Vol. 22, 1985, pp. 209-280.
[16] Délery, J., Marvin, J. G., ”Shock-Wave Boundary Layer Interactions”, AGARDograph 280, 1986, pp. 90-108.
[17] Brunet, V., Deck, S., Jacquin, L., Molton, P., “Transonic Buffet Investigations Using Experimental and DES Techniques”, 7th ONERA-DLR Aerospace Symposium ODAS 2006, Toulouse, France. ONERA-TP-2006-165, 2006.
[18] Lee, B. H. K., “Self-sustained shock oscillations on airfoils at transonic speeds”, *Progr. Aerospace Sci.*, Vol. 37, 2001, pp. 147-196.
[19] Deck, S., “Numerical Simulation of Transonic Buffet over a Supercritical Airfoil”, *AIAA J.*, Vol. 43, No. 7, 2005.
[20] Schewe, G., Knipfer, A., Mai, H., Dietz, G. Experimental and numerical investigation of nonlinear effects in transonic flutter. German Aerospace Centre internal report DLR-IB 232-2002 J 01, 2002.
[21] Finke, K., “Stoßschwingungen in schallnahen Strömungen”, VDI-Forschungsheft 580, VDI-Verlag, Düsseldorf, Germany, 1977.
[22] Raveh, D. E., Dowell, E. H., “Frequency lock-in phenomenon in oscillating airfoils in buffeting transonic flows”, International Forum on Aeroelasticity and Structural Dynamics, IFASD-2009-135, 2009.
[23] Dussauge, J.-P., Dupont, P., Debiève, J.-F., „Unsteadyness in shock wave boundary layer interactions with separation“,*Aerospace Science and Technology*, Vol. 10, 2006, pp 85-91.
[24] Xiao, Q., Tsai, H. M., “Numerical Study of Transonic Buffet on a Supercritical Airfoil”, *AIAA J.*, Vol. 44, No. 3, 2006, pp. 620-628.
[25] Geissler, W., “Numerical study of buffet and transonic flutter on the NLR 7301 airfoil”, *Aerospace Science and Technology*, Vol. 7, 2003, pp. 540-550.
[26] Pearcey, H. H., Osborne, J., Haines, A. B., **“**The Interaction between Local Effects at the Shock and Rear Separation - A Source of Significant Scale Effects in Wind-Tunnel Tests on Aerofoils and Wings”, Transonic Aerodynamics, AGARD-CP-35, 1968, pp. 11-1 - 11-23.
[27] Tijdeman, H., “Investigation on the Transonic Flow around Oscillating Airfoils”, PhD Thesis, NLR TR 77090 U, TU Delft, The Netherlands, 1977.
[28] Tichy, L., “Transsonische Strömungen an einem schwingenden Profil und deren Einfluß auf die Flattergrenze”, Dissertation, Technische Universität München, DLR Fachbericht 92-08, 1992.
[29] Schewe, G., Mai, H., Dietz, G., “Nonlinear Effects in Transonic Flutter with Emphasis on Manifestations of Limit Cycle Oscillations”, *J. Fluids Structures*, Vol. 18, 2003, pp. 3-22.